J Electroceram
DOI 10.1007/s10832-016-0040-3

Photoluminescence and ESR identification of γ-ray irradiation induced defects responsible for thermoluminescence in Tb^{3+} activated hibonite ($CaAl_{12}O_{19}$) powder material

Vijay Singh[1] · S. Watanabe[2] · T. K. Gundu Rao[2] · N. Singh[1] · Anoop K. Srivastava[3] · Pramod K. Singh[4] · H. Gao[1] · P. Mardina[1] · S. J. Dhoble[5]

Received: 26 October 2015 / Accepted: 5 May 2016

Abstract $CaAl_{12}O_{19}$ powder activated with Tb ions has been prepared by the urea combustion route. Phase evolution of the powder is determined by X-ray diffraction techniques. Photoluminescence emission of $CaAl_{12}O_{19}$:Tb consists of a dominant peak at 544 nm when excited with UV radiations. Thermoluminescence (TL) peaks at approximately 140 °C, 245 °C and 458 °C are observed in the $CaAl_{12}O_{19}$:Tb phosphor. Investigations using the technique of electron spin resonance (ESR) were carried out to study the defect centers induced in the phosphor by γ-ray irradiation. ESR study reveals the presence of several distinct centers. One of the centers (center I) with an isotropic g factor 2.0110 is tentatively assigned to an intrinsic O^- type center and this center relates with the TL peak at 140 °C. Center II with an axially symmetric g-tensor with principal values $g_{\|} = 2.0324$ and $g_{\perp} = 2.0060$ is attributable to an O_2^- ion and also appears to correlate with the 140 °C TL peak. Several F^+-centers have been identified and their correlation with the observed TL peaks will be discussed.

✉ Vijay Singh
vijayjiin2006@yahoo.com

[1] Department of Chemical Engineering, Konkuk University, Seoul 143-701, South Korea

[2] Institute of Physics, University of Sao Paulo, São Paulo 05508-090, Brazil

[3] Division of Electronics Engineering, Chonbuk National University, Jeonju, Jeonbuk 561-756, South Korea

[4] Materials Research Laboratory, Sharda University, Greater Noida 201310, India

[5] Department of Physics, RTM Nagpur University, Nagpur 440033, India

Keywords Tb^{3+} · Hibonite · Defect centers · Luminescence, electron spin resonance

1 Introduction

$CaAl_{12}O_{19}$ is known as hibonite mineral which crystallizes in the hexagonal system [1–3]. $CaAl_{12}O_{19}$ has magnetoplumbite structure containing Al_2O_3 spinel-blocks and conduction layers. Calcium is situated in the cleavage plane located between the blocks [1–5]. Due to high elastic modulus, excellent thermal shock resistance, high chemical stability, high thermal stability, and good colour-rendering index, nanocrystalline calcium aluminate compounds are being used as promising materials in new potential applications [2–7]. Calcium hexaaluminate is an oxide based fiber-reinforced ceramic matrix composite [8]. Iglesia et al. [9] investigated the influence of different parameters on calcium hexaluminate reaction sintering by spark plasma. Chandradass et al. [10] reported the synthesis of calcium hexaaluminate via reverse micelle process. For the next generation of lighting products, many efforts are being made in order to obtain light of sunlight spectrum from LEDs in the visible region. There is a need to develop new phosphors which are indispensable for white LEDs and have the remarkable luminescence enhancement. Murata et al. [6] reported the fluorescence properties of Mn^{4+} in $CaAl_{12}O_{19}$ compounds as red emitting phosphor for white LED. Absorption and photoluminescence properties of red emitting $CaAl_{12}O_{19}$:Mn^{4+} have been investigated by Brik et al. [11]. Infrared and visible upconversion emission investigations of $CaAl_{12}O_{19}$ powders doped with Er^{3+}, Yb^{3+} and Mg^{2+} ions, have been reported by Singh et al. [12]. It is to be noted that Eu^{2+} doped alkaline earth aluminates are more studied as compared to other trivalent rare earths ion doped luminescent material and an extensive spectroscopic study of this

Published online: 12 May 2016

ion does exist [13–15]. However, Tb^{3+} doped alkaline earth aluminates are scarcely studied as compared to other hosts and an extensive spectroscopic study does not exist particularly in $CaAl_{12}O_{19}$ host. Keeping in view of this and due to great demand of green-emitting phosphors, in the present investigation, we have prepared terbium activated hibonite ($CaAl_{12}O_{19}$) powder material.

Thermoluminescence (TL) is a well-known phenomenon widely applied in the field of radiation dosimetry, dating in archaeology and study of defects [16–18]. It is well established that inorganic phosphors can show efficient TL in the presence of certain suitable dopants, particularly rare earths, in the lattice [17–19]. One of the most important of these ions is trivalent terbium (Tb^{3+}) as it has been commonly employed as a green-emitting activator because of the efficient emission originating from the $^5D_4$-^7F_J transitions [20]. A number of publications related to the TL and electron spin resonance (ESR) properties of Tb^{3+} doped materials have been investigated [21–24]. An investigation of the ESR spectra and the TL glow curves of rare earth doped complex oxides samples irradiated by gamma rays was carried out by many researcher [21–27]. The results of ESR and TL in gamma-irradiated alkaline earth aluminates samples were used to analyse the mechanisms of radiation effects in aluminates [27–29].

In the present paper, we have carried out a photoluminescence study of the terbium activated $CaAl_{12}O_{19}$ powder material. In addition, the system was investigated for its thermally luminescence (TL) behavior on gamma irradiation. The defect centers created by ionizing radiations, such as alpha, beta and gamma are responsible for TL in the phosphor. To determine the chemical nature of the defect centers, ESR technique was used. In this context, ESR provides a convenient and sensitive technique for such a study. By the help of ESR-TL correlation, a possible mechanism for the glow peak is proposed.

2 Materials preparation and analysis

The terbium activated $CaAl_{12}O_{19}$ powder phosphor was prepared by solution-combustion method at an initiating temperature of 500 °C. The starting chemicals used for preparing the samples included aluminum nitrate nonahydrate (5 g of $Al(NO_3)_3\ 9H_2O$), calcium nitrate tetrahydrate (0.2570 g of $Ca(NO_3)_2\ 4H_2O$), tetraterbium heptaoxide (0.0041 g of Tb_4O_7) and urea (2.1127 g of NH_2CONH_2). All of the starting chemicals employed in the preparation were of analytical grade. Initially, aluminum nitrate, calcium nitrate, terbium oxide and urea were mixed and dissolved in deionized water in a crucible at room temperature. After ensuring the mixture was homogeneous by stirring for few minutes, a solution was obtained. Finally, the crucible with the mixture was transferred to a muffle furnace preheated to 500 °C. As the ignition occurred, the flame-producing reaction went on vigorously for few seconds. The whole process was over within 5 min. After cooling to room temperature naturally, the fluffy product was collected, and then it was ground using a pestle and mortar to make a fine powder. This resulting dry powder sample was utilized without any further treatments.

The crystal phase of the prepared phosphors was analysed by an X-ray diffraction pattern measured using X'Pert PRO-MRD, made in Netherlands. Luminescence and luminescence excitation spectra were recorded using a Fluorolog 3–22 spectrometer (Jobin Yvon) with a 450 W xenon lamp as an excitation source. A Bruker EMX ESR spectrometer operating at X-band frequency with 100 kHz modulation frequency was utilized for Electron Spin Resonance experiments. The *g*-factors of defect centers were calibrated using Diphenyl Picryl Hydrazyl (DPPH) as a standard sample. Temperature dependence of the ESR spectra was studied using a Bruker BVT 2000 variable temperature accessory. TL measurements of irradiated samples have been carried out on a Thermo Scientific 4500 TL reader. A calibrated ^{60}Co source was used for irradiating the phosphor samples to gamma rays.

3 Results and discussion

3.1 X-ray diffraction

The XRD pattern of the Tb activated $CaAl_{12}O_{19}$ phosphor is shown in Fig. 1. The pattern matched with the JCPDS standard pattern no-07-0085 corresponding to the hexagonal phase of $CaAl_{12}O_{19}$ compound. No other impurity phases were detected in the sample. It should be noticed that the furnace temperature is much lower than that required to synthesize the $CaAl_{12}O_{19}$ phase using the conventional solid-state reaction method.

3.2 Photoluminescence studies

The excitation spectrum of Tb activated $CaAl_{12}O_{19}$ phosphor is shown in Fig. 2(a). This excitation spectrum of the sample

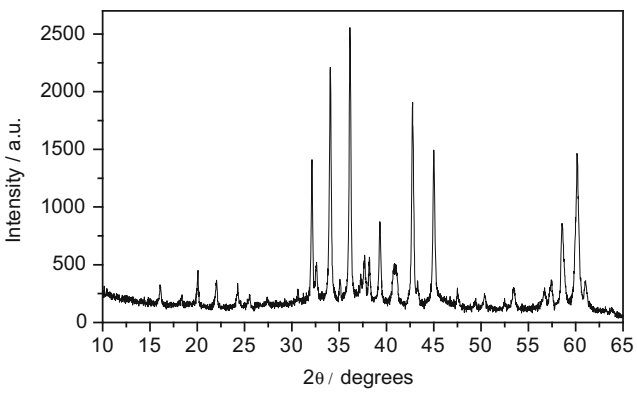

Fig. 1 XRD pattern of $CaAl_{12}O_{19}$:Tb^{3+} phosphor

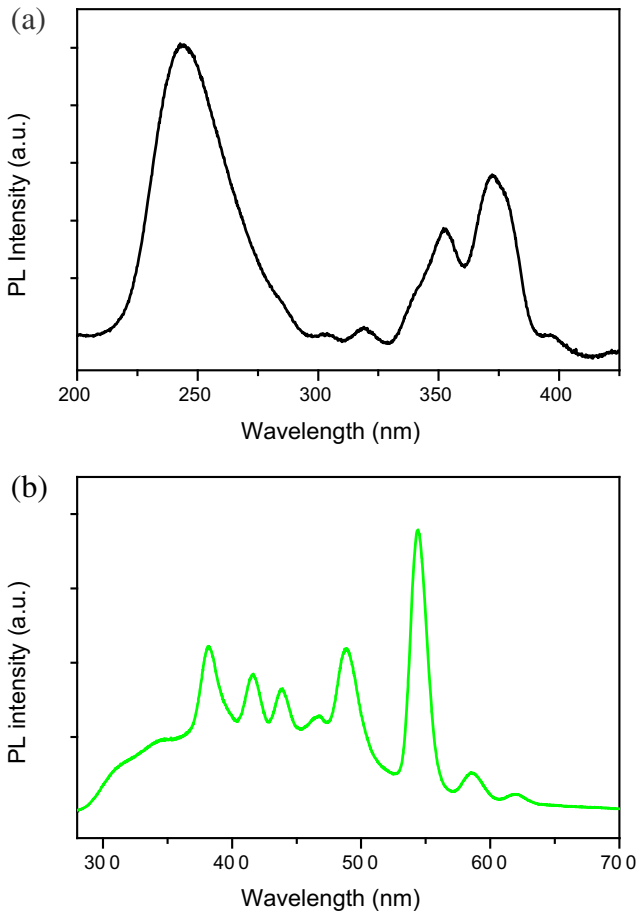

Fig. 2 (**a**) Excitation spectrum of $CaAl_{12}O_{19}:Tb^{3+}$ phosphor (λ_{emi} = 544 nm), and (**b**) Emission spectrum of $CaAl_{12}O_{19}:Tb^{3+}$ phosphor (λ_{exc} = 244 nm)

was recorded by monitoring the strongest 544 nm emission peak. The excitation spectrum is a combination of a broad band and several narrow peaks. The excitation spectrum consists of six bands located at 244, 303, 319, 352, 372 and 397 nm. The shorter wavelength peak (244 nm) was due to spin allowed $^4f_8$-$^4f_7$5d transition of Tb^{3+} ion and longer wavelengths (303, 319, 352, 372 and 397 nm) were due to spin forbidden f-f transitions [30]. The emission spectrum of Tb activated $CaAl_{12}O_{19}$ phosphor is shown in Fig. 2(b). Under 244 nm UV excitation, the intense luminescence of Tb^{3+} ion consists of a series of bands in the region 350–650 nm. The emission bands located at 382, 416, 438 and 468 nm correspond to the $^5D_3$ - ^7F_J (J = 6, 5, 4 and 3) transitions, respectively. Another set of emission bands peaked at 488, 544, 585 and 620 nm belong to the $^5D_4$-^7F_J (J = 6, 5, 4 and 3) transitions. The green emission transition $^5D_4$-$^7F_5$ (544 nm) is dominant among these transitions. The result indicates that Tb^{3+} ions have successfully entered into the $CaAl_{12}O_{19}$ host. Further, it is well known that rare-earth ion activated phosphor (not blank) have excellent optical and dosimetric properties. Therefore, in the next section, we have focused on TL and ESR investigations on Tb activated $CaAl_{12}O_{19}$ phosphor in order to identify the role of the radiation induced radical ions/paramagnetic ions in the TL process. Gamma-irradiation was used to create electron/hole traps and also to investigate the role of oxygen defects in the optical properties. Radiation induced defects in Tb^{3+} activated phosphor systems have also been previously studied by using TL and ESR techniques [23, 27, 31].

3.3 TL and ESR studies

$CaAl_{12}O_{19}$:Tb exhibits three TL glow peaks at approximately 140 °C, 245 °C and 458 °C after gamma irradiation (dose: 50 Gy). The main glow peak is observed at 458 °C and the other two peaks are relatively smaller. The glow curve is shown in Fig. 3. The glow curves for the samples were obtained at a heating rate of 4 °C/s.

Gamma irradiation induces defect centers in the phosphor and the resulting room temperature ESR spectrum after irradiation is shown in Fig. 4. Experiments on the phosphor which was subjected to annealing at different high temperature point to the presence of several defect centers. The ESR lines associated with these centers are labeled in Fig. 4.

Calcium hexaaluminate ($CaAl_{12}O_{19}$) occurs in nature as the mineral hibonite and exhibits a magnetoplumbite-type structure with space group $P6_3/mmc$ with Z = 2 [32]. The structure is dominated by polyhedral layers perpendicular to the c-axis, in which Ca occupies a 12-coordinated polyhedron, and Al^{3+} is distributed over five M sites, M1 is a regular octahedron (D_{3d}), M2 is a trigonal bipyramid with an ideal site symmetry of D_{3h}, M3 is a tetrahedron (C_{3v}), M4 is a trigonally distorted octahedron (C_{3v}) and M5 is a strongly distorted octahedron (C_3). The multiplicity of the cation sites and their coordination numbers may be summarized as follows: $^{[12]}$:Ca, $^{[6]}$M1, $^{[5]}$M2, $^{[4]}M3_2$, $^{[6]}M4_2$, $^{[6]}M5_6O_{19}$ (where coordination numbers are

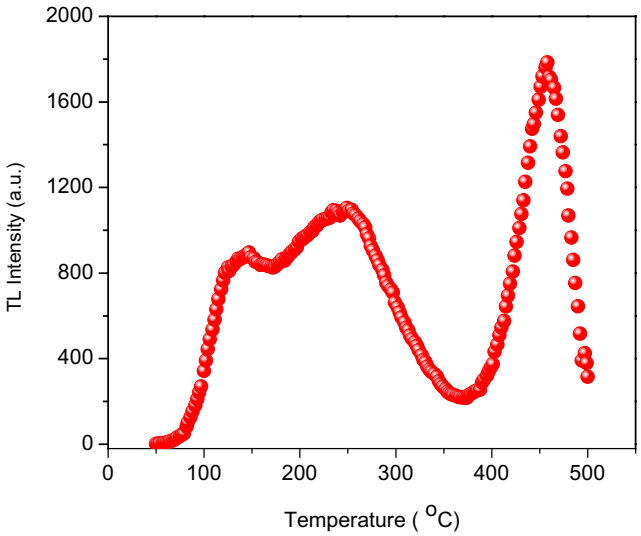

Fig. 3 TL glow curve of $CaAl_{12}O_{19}$:Tb at 4 °C/s for 50 Gy dose showing TL peaks at 140 °C, 245 °C and 458 °C

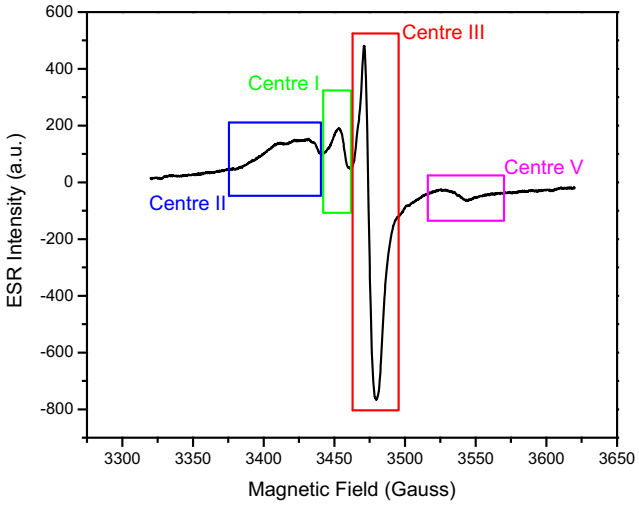

Fig. 4 ESR spectrum at room temperature of irradiated $CaAl_{12}O_{19}$:Tb phosphor (gamma dose: 10 kGy). Line labeled as I is due to an O^- ion. Center II line is assigned to an O_2^- ion and center III is attributed to an F^+ center. Center V line is from an F^+ center exhibiting an axial g-tensor

superscripted in square brackets and the multiplicity of the site is subscripted). There are spinel blocks with Al^{3+} in both tetrahedral and octahedral sites bound with intermediate mirror layers containing large cations.

Antisite cation exchange is probable in $CaAl_{12}O_{19}$ wherein Al atoms will partially replace Ca sites. Such replacement, called as cation exchange disorder, is a point defect in crystal lattices involving exchange of cation positions. The presence of such defects affects the chemical properties of the phosphor. Theoretical calculations have predicted the occurrence of such defects [33]. Their presence has been confirmed by X-ray diffraction [34], X-ray absorption fine structure [35] and direct observation by high-angle annular dark-field and annual bright-field scanning transmission electron microscopy [36]. Luminescence properties are also affected by cation exchange disorder and an example is provided by a recent study of Cr^{3+} doped AB_2O_4 spinel compounds [37]. The site of Ca^{2+} ion in $CaAl_{12}O_{19}$ has D_{3h} symmetry with 12-fold coordination and the ionic radius of calcium ion is 1.34 Å in this coordination [38]. Al^{3+} ion has 0.39 Å, 0.535 Å and 0.48 Å ionic radii in octahedral, tetrahedral and five-fold coordinated sites respectively. Since the ionic radius of Tb^{3+} ion is 1.095 Å in 9-fold coordinated site, it is expected that it would substitute Ca^{2+} ion. It may be mentioned that Merkle et al. [39] have pointed out that rare-earth ions occupy Ca^{2+} sites in $CaAl_{12}O_{19}$ lattice. The replacement of divalent calcium ions by trivalent terbium leads to excess net positive charge and the charge balance could be achieved by formation of calcium vacancies or extra O^{2-} ions at nearby interstitial positions. Several trapping sites for the electron and hole on irradiation are created due to antisite formation which results from the interchange of the ions in the octahedral, tetrahedral positions and trigonal bipyramid positions by divalent and trivalent ions. Also centers created from defects and impurities present in the lattice have the possibility of affecting the luminescent and optical properties of the phosphor.

The center related to line I in Fig. 4 has an isotropic g-value equal to 2.0115 and 11 gauss line width. The ESR line is relatively broad and indicates a possible unresolved hyperfine structure. The unresolved structure results from the interaction of the unpaired electron with nearby nuclear spins. Calcium as well as aluminum in $CaAl_{12}O_{19}$ have isotopes with nuclear spins 7/2 and 5/2: ^{43}Ca and ^{27}Al. ^{27}Al is more abundant (100 %) than ^{43}Ca (0.14 %) and its nuclear magnetic moment is higher (3.64) than that of ^{43}Ca (−1.32) [40]. It is likely, therefore, that the electronic spin will be interacting with aluminum ions due to its larger abundance. It is known that the cation disorder and non-stoichiometry of oxides provide a number of lattice defects which may serve as trapping centers. First principle calculations have shown that oxygen vacancies would more easily form with cation disorder than in a perfect cation-ordered system [41]. In this environment in the lattice, oxygen vacancies should lead to F^+ − centers by trapping electrons. On the other hand, hole trapping at calcium and magnesium vacancies can lead to formation of V-centers [42]. The observed ESR line of center I and the associated unresolved hyperfine structure indicates that the unpaired electron is slightly delocalized and interacts with nearby aluminum nuclei. Konstantinov et al. [43] envisage the charges in oxides to be trapped near double or more charged defects which will enable the charge to be delocalized to give stability. This delocalization also allows the charge to interact with the surrounding nuclei. Hence centre I is tentatively assigned to a V-centre -a hole trapped on an oxygen ion, forming an O^- ion, adjacent to an Ca-ion/Al-ion vacancy. The positive g-shift in the principal g-value of center I is in accordance with the model of a hole trapped in a p_z orbital on an oxygen ion. The features of center I ESR line are similar to those observed by Ibarra et al. [44] in $MgAl_2O_4$. Ibarra et al. carried out optical absorption measurements and ESR studies on $MgAl_2O_4$ spinel. On X-irradiation of the spinel, an ESR spectrum was observed with g = 2.011. After taking into consideration the optical absorption spectra, they concluded that the ESR spectra is related to hole trapping at cation vacancies i.e., to V-type centers formed by hole trapping at oxygen ions surrounding cation vacancies. In $CaAl_{12}O_{19}$:Tb, the stability of center I was measured using a pulsed-thermal annealing method. After heating the sample up to a given temperature, where it is maintained for 3 min, it is cooled rapidly down to room temperature for ESR measurements. The thermal annealing behavior of center I is shown in Fig. 5. It is seen that the center becomes unstable around 70 °C and decays in the temperature range 70–250 °C. This decay appears to relate to the TL peak at 140 °C.

Hyperfine splitting is not observed for the center associated with line II shown in Fig. 4 and the center is characterized by

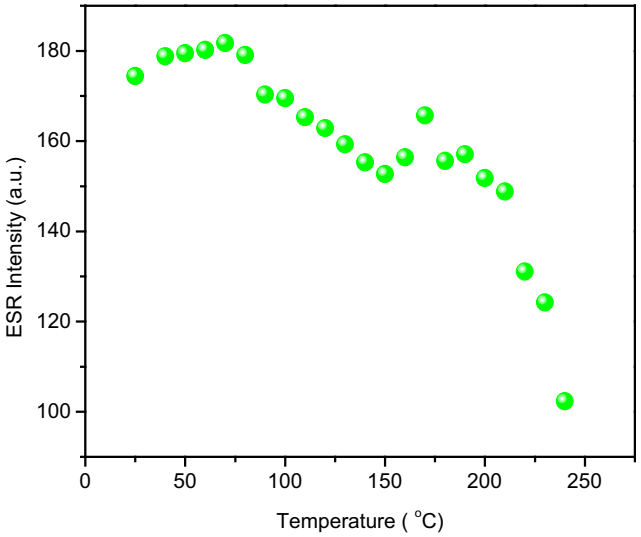

Fig. 5 Thermal annealing behaviour of center I in $CaAl_{12}O_{19}$:Tb phosphor

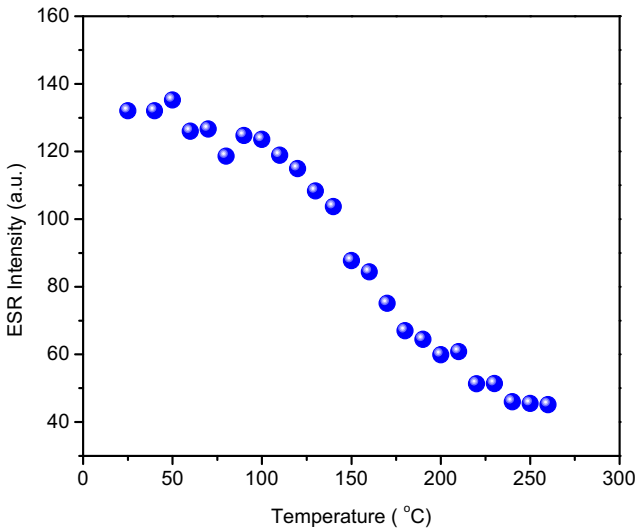

Fig. 6 Thermal annealing behaviour of center II in $CaAl_{12}O_{19}$:Tb phosphor

an axially symmetric *g*-tensor with principal values $g_{\|} = 2.0283$ and $g_{\perp} = 2.0058$. Irradiation with gamma rays, in general, leads to the formation of V-centers, F-centers and F^+ – centers (an electron trapped at an anion vacancy) in oxide systems [45]. An anion radical like superoxide O_2^- ion is also known to form in oxides particularly on their surfaces and ESR has been extremely helpful in identifying the formation of superoxide ion. A simple explanation for the formation is to involve the direct transfer of an electron from the oxide surface to an adsorbed oxygen molecule. In this context, Garrone et al. [46] have suggested an alternate pathway to O_2^- formation in oxide systems and this involves the production through the agency of anion intermediates. They observe the superoxide ion to be characterized by an axial *g*-tensor with principal values $g_{\|} = 2.070$ and $g_{\perp} = 2.008$ in their study on MgO. O_2^- ions with considerable *g*-anisotropy have also been observed in a number of zeolites and metal oxides [47–49]. It is noteworthy that the $g_{\|}$ value for the O_2^- ion was found to be highly matrix dependent and ranged between 2.015 and 2.080 and is controlled by the magnitude of the crystal-field from the cations. On the other hand, $g_{\perp}$ is expected to be relatively close to free-electron value. Based on these results, centre II with a relatively large anisotropy in *g*-values in the present system is tentatively assigned to an O_2^- ion. The thermal annealing behavior of center II is shown in Fig. 6. It is observed that the center becomes unstable around 100 °C and decays in the broad temperature range 100–240 °C. Hence, O_2^- ion could also be associated with the 140 °C TL peak along with O^- ion.

The line labeled as center III in Fig. 4 is due to a centre characterized by a single ESR line with an isotropic g-value equal to 2.0021 and 7 gauss linewidth. During irradiation, oxygen ion vacancies may trap electrons resulting in the formation of F^+ centers. The earliest system in which F center (an electron trapped at the F^- ion vacancy) was observed is LiF [50]. In this alkali halide system the center exhibited an unusually large linewidth of about 100 gauss and a g-value close to the free- spin value. On the other hand, F^+ centre has a linewidth of about 1 gauss in MgO system [51] and this linewidth is the inherent linewidth of the center. The ions present in a system determine the linewidth (whether they have nuclei with magnetic moment and their abundance) and more importantly on the delocalization of the unpaired electron which depends on the host lattice. In alkali halides, the unpaired electron is considerably delocalized and interacts with several alkali and halide ions from successive neighboring shells. For example, the observed linewidth in KCl is around 20 gauss [52] and in LiCl it is 58 gauss [52]. In a system like BaO [53], the linewidth of F^+ center is about 3.5 gauss. Apart from alkali halides, centers with an electon trapped at an anion vacancy (i.e., F^+ centers) have also been observed in oxide systems. In all these systems, g-values are found to be close the free-electron value with a g-shift which may be positive or negative. A recent observation of this center is in pure and defective TiO_2 nanoparticles [54]. In the present case of center III, linewidth is not large and the g-shift is small. Based on these observations, center III is tentatively assigned to an F^+-center. Fig. 7 shows the thermal annealing behavior of center III. It is observed that the intensity of the ESR line associated with this center decreases in the temperature range from about 60 °C to around 300 °C. The decay of center III appears to encompass the region of the two low temperature TL peaks and thus could be the recombination center associated with 140 °C and 245 °C TL peaks.

During the course of thermal annealing experiments, a new ESR line was visible after the decay of center III at almost the same position of center III line. It appears that the new line is present in the room temperature spectrum after irradiation. However, it is not visible due to overlap from the relatively

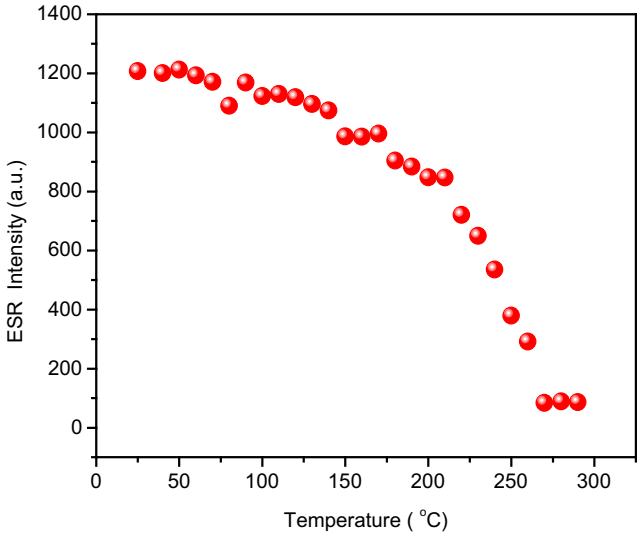

Fig. 7 Thermal annealing behaviour of center III in $CaAl_{12}O_{19}$:Tb phosphor

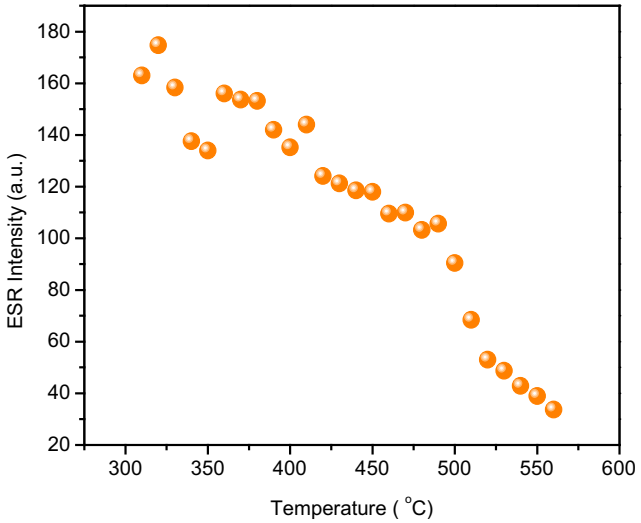

Fig. 9 Thermal annealing behaviour of center IV in $CaAl_{12}O_{19}$:Tb phosphor

strong line associated with center III. The ESR spectrum after thermal anneal at 320 °C is shown in Fig. 8 and the new line is labeled as center IV. The associated defect center has an isotropic g value of 2.0040 with 8 gauss linewidth. This centre (IV) is also tentatively assigned to an F^+-centre based on the reasons mentioned earlier. The thermal annealing result of this center from the temperature where it is visible is shown in Fig. 9. It is seen that the intensity of the ESR line decreases in the temperature range from about 300 °C to around 550 °C. The center thus has the possibility of being associated with the high temperature TL peak at 458 °C.

The ESR lines associated with center V are shown in Fig. 4. This center is characterized by an axially symmetric g-tensor with principal values $g_{\parallel} = 1.9721$ and $g_{\perp} = 1.9654$. Similar g-values are also observed in $CaZrO_3$:Tb [23] and yttria stabilized zirconia (YSZ), i.e. ZrO_2:Y [55]. In YSZ, the principal g-values are $g_{\parallel} = 1.996$ and $g_{\perp} = 1.972$. The g-values are observed to be smaller than the free-electron value. These centers in these systems were identified as F^+-centers. F^+-centers normally exhibit isotropic g-values and the assignment in YSZ was interpreted by invoking the presence of a symmetry breaking defect at an anionic site near the F^+-center which explains the axial nature of the g-tensor. The symmetry breaking defect was considered to be the neutral F-center (oxygen vacancy with two electrons) which has a high probability of formation in YSZ lattice owing to the presence of a large density of oxygen vacancies in this system. Center V in the present system is also identified as an F^+-center and the center needs to be in the vicinity of an F -center which results in the observed features. Oxygen vacancies may be present in $CaAl_{12}O_{19}$ lattice due to reasons mentioned earlier. Irradiation can then lead to the formation of F -center in close proximity to center V. With reference to the present study, it may be mentioned that an F^+-center in X-irradiated sodium β-alumina also exhibits an axial g-tensor with principal values $g_{\parallel} = 2.0076$ and $g_{\perp} = 2.0032$ [56]. It is to be noted that the g-shifts are positive in this system. Fig. 10 shows the thermal annealing behavior of centre V. It is observed that the centre becomes unstable around 40 °C and decays in the broad temperature range 40–260 °C. It appears that the axial F^+ center is also related to the 140 °C TL peak along with O^- ion.

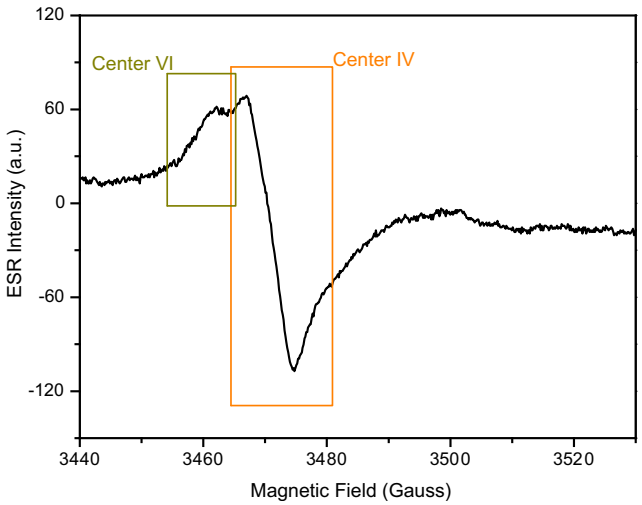

Fig. 8 ESR spectrum at room temperature of irradiated $CaAl_{12}O_{19}$:Tb phosphor after thermal anneal at 320 °C. Center IV and center VI lines are attributed to F^+ centers

An observation of Fig. 8 shows an additional ESR line apart from the line assigned to centre IV. This line is broader and can be seen as a shoulder on the left portion of center IV ESR line. The related defect center is characterized by an isotropic g value of 2.0047 with 14 gauss line width. This center (VI) is also tentatively assigned to an F^+-center. The results of thermal annealing experiments are shown in Fig. 11. The center exhibits two stages of decay. The first stage starts

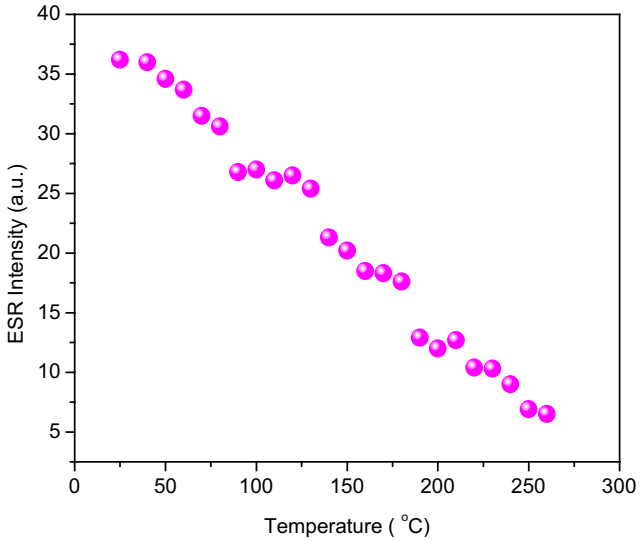

Fig. 10 Thermal annealing behaviour of center V in $CaAl_{12}O_{19}$:Tb phosphor

from about 260 °C and continues till 350 °C. It is stable in the region 350 °C–450 °C and the final stage of decay is found to be in the region 450–560 °C. Though it appears that centre VI could be associated with 245 °C TL peak, the results are not definitive as it is difficult to observe and follow the decay of the center in temperature region below 250 °C due to the presence of strong ESR line from center III. Essentially no specific TL role could be assigned for this F^+ center. A general comment may be made about the several F^+ centers observed in the present study. The crystal structure of $CaAl_{12}O_{19}$ shows a multiplicity of cation sties and likewise a number of oxygen sites differing in their environment and site locations also exist in the phosphor. Therefore, one may expect an electron trapped at different anion vacancies to lead to the formation of several F^+ centers with different thermal stabilities. The observed F^+ centers in the phosphor are perhaps a reflection of these expectations.

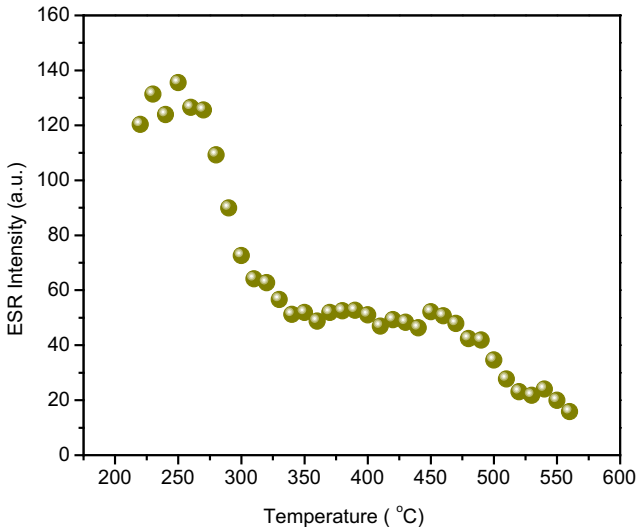

Fig. 11 Thermal annealing behaviour of center VI in $CaAl_{12}O_{19}$:Tb phosphor

Rare earth ions present as dopants in certain materials lead to efficient thermoluminescence. With terbium as a dopant in the present phosphor, $CaAl_{12}O_{19}$:Tb also exhibits such thermoluminescence. Based on the present ESR and TL results, a TL mechanism is suggested for the $CaAl_{12}O_{19}$:Tb phosphor. Holes released from O^- and O_2^- ions during TL readout recombine with the electrons trapped at anion vacancies (centre III) leading to the formation of Tb^{3+} ions in an excited state. The excited Tb^{3+} ion gives its characteristic emission during the de-excitation process. The following mechanism may be proposed for the observed TL peaks based on the present observations.

On gamma irradiation:

$$CaAl_{12}O_{19}:Tb \rightarrow O^- \text{ ions}, O_2^- \text{ ions}, F^+ \text{ centers},$$

On heating the sample during TL experiments:

$$O^- \rightarrow O^{2-} + h$$

$$(h + F^+) + Tb^{3+} \rightarrow \left\{(Tb^{3+})^*\right\}$$

$$\left\{(Tb^{3+})^*\right\} \rightarrow Tb^{3+} + h\nu \text{ (TL emission at 140 °C)}$$

$$O_2^- \rightarrow O_2^{2-} + h$$

$$(h + F^+) + Tb^{3+} \rightarrow \left\{(Tb^{3+})^*\right\}$$

$$\left\{(Tb^{3+})^*\right\} \rightarrow Tb^{3+} + h\nu \text{ (TL emission at 140 °C)}$$

$$[h \text{ (holes released from unknown traps)} + F^+] + Tb^{3+} \rightarrow \left\{(Tb^{3+})^*\right\}$$

$$\left\{(Tb^{3+})^*\right\} \rightarrow Tb^{3+} + h\nu \text{ (TL emission at 245 °C)}$$

4 Conclusions

Tb activated $CaAl_{12}O_{19}$ phosphor powder was synthesized using a fast, very simple and one-step combustion method. The XRD results confirmed that the crystalline hexagonal structure of $CaAl_{12}O_{19}$ could be obtained by the economical viable synthesis method. A dominant green emission peak at 544 nm ($^5D_4$-$^7F_5$) was observed from the $CaAl_{12}O_{19}$:Tb powder phosphor under 244 nm excitation. Thermoluminescence peaks at 140 °C, 245 °C and 458 °C are observed in the $CaAl_{12}O_{19}$:Tb phosphor for a heating rate of 4 °C/s with 458 °C peak being the dominant peak. Several defect centers have been identified in the irradiated phosphor and these are tentatively assigned to an O^- ion, O_2^- ion and F^+ centers. The superoxide ion O_2^- and the O^- ion are found to correlate with the low temperature TL peak at140 °C. One of the F^+ centres (centre III) is associated

with the 245 °C peak whilst the second F^+ centre (centre IV) is related to the high temperature TL peak at 458 °C. The perturbed F^+ centre (Centre V) with axial principal g-values appears to be related to the TL peak at 140 °C. No specific TL role could be attributed to the F^+ center associated with center VI.

Acknowledgments This paper was supported by the KU Research Professor Program of Konkuk University. T. K. Gundu Rao is grateful to CAPES, Brazil for the research fellowship.

References

1. J. M. P. J. Verstegen, A. L. N. Stevels, J. Lumin. **9**, 406 (1974)
2. H. S. Jeon, S. K. Kim, S. C. Kim, S. H. Park, S. I. Mho, H. L. Park, Solid State Commun. **102**, 555 (1997)
3. V. Singh, R. P. S. Chakradhar, J. L. Rao, D.-K. Kim, Solid State Sci. **10**, 1525 (2008)
4. M. Nagashima, T. Armbruster, T. Hainschwang, Mineral. Mag. **74**, 871 (2010)
5. K. Kato, H. Saalfeld, N. Jb. Mineral. (Abh.) **109**, 192 (1968)
6. T. Murata, T. Tanoue, M. Iwasaki, K. Morinaga, T. Hase, J. Lumin. **114**, 207 (2005)
7. Z. G. Nie, J. H. Zhang, X. Zhang, S. Z. Lü, X. G. Ren, G. B. Zhang, X. J. Wang, J. Solid State Chem. **180**, 2933 (2007)
8. T. A. Parthasarathy, E. Boakye, M. K. Cinibulk, M. D. Petry, J. Am. Ceram. Soc. **82**, 3575 (1999)
9. P. G. De La Iglesia, O. García-Moreno, R. Torrecillas, J. L. Menéndez, Ceram. Int. **38**, 5325 (2012)
10. J. Chandradass, D. S. Bae, K. H. Kim, J. Non-Cryst. Solids **355**, 2429 (2009)
11. M. G. Brik, Y. X. Pan, G. K. Liu, J. Alloys Compd. **509**, 1452 (2011)
12. V. Singh, V. K. Rai, I.-J. Lee, I. Ledoux-Rak, K. Al-Shamery, J. Nordmann, M. Haase, Appl. Phys. B Lasers Opt. **106**, 223 (2012)
13. T. Aitasalo, J. Hölsä, H. Jungner, M. Lastusaari, J. Niittykoski, J. Alloys Compd. **341**, 76 (2002)
14. L.-T. Chen, C.-S. Hwang, I.-L. Sun, I.-G. Chen, J. Lumin. **118**, 12 (2006)
15. J. Hölsä, H. Jungner, M. Lastusaari, J. Niittykoski, J. Alloys Compd. **326**(323–324) (2001)
16. M. Duttine, P. Guibert, A. Perraut, C. Lahaye, F. Bechtel, G. Villeneuve, Radiat. Meas. **39**, 375 (2005)
17. S. Watanabe, N. F. Cano, T. K. Gundu Rao, L. M. Oliveira, L. S. Carmo, J. F. D. Chubaci, Appl. Radiat. Isot. **105**, 119 (2015)
18. B. Sanyal, V. Natarajan, S. P. Chawla, A. Sharma, Radiat. Meas. **45**, 899 (2010)
19. R. E. S. Khadijeh, A. A. Kharieky, E. Maryam, J. Rare Earths **32**, 1003 (2014)
20. P. Indira, S. Kondala Rao, K. V. R. Murthy, Optik **126**, 2390 (2015)
21. M. Kumar, S. K. Gupta, J. Lumin. **168**, 151 (2015)
22. E. Bortolin, P. Fattibene, C. Furetta, S. Onori, Appl. Radiat. Isot. **44**, 327 (1993)
23. V. Singh, S. Watanabe, T. K. Gundu Rao, K. Al-Shamery, M. Haase, Y. D. Jho, J. Lumin. **132**, 2036 (2012)
24. S. S. Sanaye, B. S. Dhabekar, R. Kumar, S. N. Menon, S. S. Shinde, T. K. Gundu Rao, B. C. Bhatt, J. Lumin. **105**, 1 (2003)
25. V. Singh, T. K. Gundu Rao, D.-K. Kim, Radiat. Meas. **43**, 1198 (2008)
26. S. J. Dhoble, S. V. Moharil, T. K. Gundu Rao, J. Lumin. **126**, 383 (2007)
27. S. Menon, B. Dhabekar, E. A. Raja, S. P. More, T. K. G. Rao, R. K. Kher, J. Lumin. **128**, 1673 (2008)
28. V. Singh, T. K. Gundu Rao, S. Watanabe, I.-J. Lee, Appl. Phys. B Lasers Opt. **104**, 1019 (2011)
29. V. Singh, S. Watanabe, T. K. Gundu Rao, J. F. D. Chubaci, H.-Y. Kwak, J. Non-Cryst. Solids **356**, 1185 (2010)
30. B. M. Manohara, H. Nagabhushana, D. V. Sunitha, K. Thyagarajan, B. D. Prasad, S. C. Sharma, B. M. Nagabhushana, R. P. S. Chakradhar, J. Alloys Compd. **592**, 319 (2014)
31. E. Alagu Raja, S. Menon, B. Dhabekar, N. S. Rawat, T. K. Gundu Rao, J. Lumin. **129**, 829 (2009)
32. A. Utsunomiya, K. Tanaka, H. Morikawa, F. Marumo, H. Kojima, J. Solid State Chem. **75**, 197 (1998)
33. M. M. Kuklja, J. Phys. Condens. Matter **12**, 2953 (2000)
34. A. P. Patel, M. R. Levy, R. W. Grimes, R. M. Gaume, R. S. Frigelson, K. J. McClellan, C. R. Stanek, Appl. Phys. Lett. **93**, 191902 (2008)
35. J. Dong, K. Lu, Phys. Rev. **43**, 8808 (1991)
36. D. Truong, M. K. Devaraju, T. Tomai, I. Honma, ACS Appl. Mater. Interfaces **5**, 9926 (2013)
37. N. Basavaraju, K. R. Priolkar, D. Gourier, S. K. Sharma, A. Bessiere, B. Viana, Phys. Chem. Chem. Phys. **17**, 1790 (2015)
38. R. D. Shannon, Acta Cryst **A32**, 751 (1976)
39. L. D. Merkle, B. Zandi, R. Moncorge, Y. Guyot, H. R. Verdun, B. McIntosh, J. Appl. Phys. **79**, 1849 (1996)
40. R. C. Weast (ed.), *Handbook of Chemistry and Physics* (CRC, Cleveland, 1971)
41. N. Yuan, X. Liu, F. Meng, D. Zhou, J. Meng, Ionics **21**, 1675 (2014)
42. M. S. Holston, J. W. McClory, N. C. Giles, L. E. Halliburton, J. Lumin. **160**, 43 (2015)
43. N. Y. Konstantinov, L. V. Karaseva, V. V. Gromov, Dokl. Acad. Nauk. SSR **228**, 631 (1980)
44. A. Ibarra, F. J. Lopez, J. de Castro, Phys. Rev. **B44**, 7256 (1991)
45. V. Singh, V. Kumar Rai, S. Watanabe, T. K. Gundu Rao, L. Badie, I. Ladoux-Rak, J. Y-D, Appl. Phys. **108**, 437 (2012)
46. E. Garrone, A. Zecchina, F. S. Stone, J. Catal. **62**, 396 (1980)
47. D. D. Eley, M. A. Zammitt, J. Catal. **21**, 366 (1971)
48. K. M. Wong, J. H. Lunsford, J. Phys. Chem. **74**, 1165 (1971)
49. J. H. Lunsford, Catal. Rev. **8**, 135 (1973)
50. C. A. Hutchison, Phys. Rev. **75**, 1769 (1949)
51. J. E. Wertz, P. Auzins, R. A. Weeks, R. H. Silsbee, Phys. Rev. **107**, 1535 (1957)
52. W. C. Holton, H. Blum, Phys. Rev. **125**, 89 (1962)
53. A. J. Tench, R. L. Nelson, Proc. Phys. Soc. **92**, 1055 (1967)
54. B. Choudhury, A. Choudhury, Sci. Adv. Mater. **6**, 2115 (2014)
55. J. M. Costantini, F. Beuneu, D. Gourier, C. Trautmann, G. Calas, M. Toulemonde, J. Phys. Condens. Matter **16**, 3957 (2004)
56. K. O'Donnell, R. C. Barklie, B. Henderson, J. Phys. C Solid State Phys. **11**, 3871 (1978)